# Gain of KL-Domain Adaptive FBP Image Reconstruction for 4-D Dynamic CT

Jing Wang, Tianfang Li, Hongbing Lu, *Member*, *IEEE*, and Zhengrong Liang*, *Fellow*, *IEEE*

***Abstract* -- Four-dimensional dynamic computed tomography (4D-dCT) plays an important role in radiation treatment planning, delivery, and verification for lung cancer management, in addition to heart studies. 4D-dCT acquires multiple repeated measurements from the same patient. Therefore, the radiation dose during a 4D-dCT procedure is much higher than a routine 3D CT study. Low-dose scans for 4D-dCT is needed. In this work, a new reconstruction strategy is proposed to address the noise problem associated with low-dose dynamic CT scans. It first applies the Karhunen-Loève (KL) transform to the neighboring phases of 4D-dCT noise sinogram to consider the data correlation along the time dimension. In the KL domain, the independent 3D principal components are arranged according to their signal-to-noise ratios (which are reflected by their eigenvalues). It then adapts the filtered backprojection (FBP) algorithm to reconstruct each principal component in the KL domain, where the filter's cutoff frequency is adaptive to the eigenvalue of the corresponding KL component. Finally, the 4D-dCT image is obtained by inverse KL transform. A patient study was performed to demonstrate the effectiveness of the proposed strategy with comparison to a direct FBP reconstruction which does not consider the correlation or employ the KL transform. The gain of the KL-domain adaptive FBP reconstruction was measured quantitatively by noise-resolution tradeoff study.**

## I. Introduction

FOUR-DIMENSIONAL dynamic computed tomography (4D-dCT) plays an important role in treatment planning for radiation therapy [1]-[3]. 4D-dCT contains information of tumor and normal organ motion. Such information can be used as input for treatment planning, delivery, and verification purposes during radiation therapy. 4D-dCT contains multiple phases of 3D-CT datasets. For example, 10 phases of 3D-CT datasets are usually acquired in treatment planning for lung cancer [1]-[3]. Thus, the radiation dose of 4D-dCT for lung imaging is about 10 times higher than that of a conventional 3D-CT study. Radiation dose during 4D-dCT procedure has raised concerns in radiotherapy community. One of the most cost-effective means to reduce radiation during CT procedures is to acquire data with less X-ray photons, or a low mAs protocol. However, the image quality will be degraded due to excessive noise and noise-induced streak artifacts [4]. Therefore, noise reduction is necessary to improve the quality of CT images acquired with low mAs protocols.

Currently, many noise reduction methods have been proposed to reduce noise presented in conventional 2D or 3D CT images acquired using lower mAs protocols. One class of these methods is based on local data characteristics. For example, Hsieh [4] utilized an adaptive trimmed mean filter to smooth detected signal with high uncertainty, which induces the steak artifacts due to photon starvation. Kachelrieβ *et. al.* [5] proposed a generalized adaptive filtering scheme to reduce noise in projection image or sinogram for both 2D fan-beam and 3D helical CT scans. Zhong *et. al.* [6] proposed a denoising algorithm based on singularity detection in wavelet domain for cone-beam breast CT imaging. Another class of these methods is based on statistical properties of the noise in the sinogram. The ideal sinogram is estimated or restored by minimizing certain objective functions which is derived from the noise model of the sinogram data. For example, La Rivière [7] proposed a sinogram smoothing algorithm based on Poisson distributed noise of the detected signal. In our previous work [8][9], we proposed a penalized weighted least-squares (PWLS) algorithm based on the first and second moments of the noise in the sinogram after data calibration (including a logarithmic transformation). These previous studies consider only the noise properties in each individual frame or phase. In 4D-dCT, the acquired data among phases are highly correlated since their 3D-CT images represent the same patient at different stages due to both voluntary and involuntary motions. If a noise reduction strategy can take into account the correlation among different phases, it is then expected to be more effective in noise treatment for 4D-dCT than a similar approach without considering the correlation.

One approach to consider the correlation among different phases is to register the reconstructed 3D-CT images at different phases using a deformable model in the image domain [10][11]. After deformable registration, the difference between two phases can be described as a field of 3D vectors.

*This work was supported in part by the NIH National Cancer Institute under Grant # CA082402. Dr. H. Lu was supported in part by the National Nature Science Foundation of China under Grant 30470490.

J. Wang was with the Department of Radiology, State University of New York, Stony Brook NY 11794 USA. He is now with Department of Radiation Oncology, Stanford University, Stanford, CA 94305 USA.

T. Li is with Department of Radiation Oncology, University of Pittsburg Medical Center, Pittsburg, PA, 15901 USA.

H. Lu is with Department of Biomedical Engineering, the Fourth Military Medical University, Xi'an, Shannxi 710032 China.

Z. Liang is with the Department of Radiology, State University of New York, Stony Brook, NY 11794 USA (jzl@mil.sunysb.edu).

Then the noise reduction for a certain phase (or image) can borrow information from other phases through the deformable fields. Such image-domain approach has been implemented to reduce noise in helical 4D-dCT and improved image quality was observed [10][11].

An alternative approach to consider the correlations among different phases of 4D-dCT is to utilize the principal component analysis or the Karhunen-Loève (KL) transform. By applying the KL transform among different phases, the 4D-dCT sinogram is decomposed into a series of independent 3D KL principal components. These KL components are arranged according to their eigenvalues. The eigenvalue of each KL component reflects the intrinsic signal-to-noise ratio (SNR) of that component. Therefore, the KL transform provides an elegant way to consider the correlation between different phases. Such sinogram-domain approach has been explored in nuclear medicine cardiac imaging [12]-[15]. A drawback in these previous efforts is related to the motion during the entire cycle of the heart beats. A single KL transform for the entire phases may not be an optimal approach to consider the correlation which is strongest among the nearest phases. Two phases with a larger separate distance would have less similarity or less correlation.

In this work, we adapt the alternative sinogram-domain approach and apply the KL transform among the nearest phases instead of all the phases. Furthermore, rather than discarding the higher order KL components as used in [12]-[14] for noise reduction, all the KL components are treated by a noise filter which is adaptive to their eigenvalues or SNRs. To remain computing efficiency in 4D-dCT studies, the well-established filtered backprojection (FBP) reconstruction is adapted and implemented in the KL domain, where the adaptive filtering is realized by allowing the cutoff frequency to be adaptive to the KL eigenvalue.

## II. Methods

An obtained 4D-dCT sinogram consists of a series of 3D-CT projection datasets, which can be acquired by either step-shot mode or spiral mode at different times or phases during a lung-breathing or heart-beating cycle. Given a phase, its nearest neighbors are the two phases, one was acquired before and the other was acquired after itself. These two nearest neighbors have the strongest correlation with the concerned phase. In this study, the KL transform was first applied to these two nearest neighboring phases and the concerned phase. The KL transform on the selected three phases' sinograms $y$ can be described by

$$\tilde{y} = A\, y \tag{1}$$

where $A$ is the KL transform matrix and can be determined by the data itself according to the following equation

$$K_t A^T = A^T D \tag{2}$$

where $K_t$ is the covariance matrix of the selected phases' 3D sinograms and $D$ is a diagonal matrix with elements being the KL eigenvalues $\{ d_l \}$, $l = 1, 2, 3$ . The covariance matrix $K_t$ can be calculated by

$$[K_t]_{kl} = \frac{1}{N-1} \sum_{i=1}^{N} (y_{i,k} - \bar{y}_k)(y_{i,l} - \bar{y}_l) . \tag{3}$$

In equation (3), $y_{i,k}$ is the *i*-th projection datum within *k*-th phase, $\bar{y}_k$ is the mean value of the projection data in phase *k*, and $N$ is the total number of the projection data within each phase.

If the 4D-dCT sinogram consists of ten phases, the KL transform of equations (1)-(3) will be applied ten times, one time for each phase. For each KL transform on a concerned phase and its two nearest neighbors, three principal components will be generated in the KL domain. Each KL component has a SNR strongly depending on its KL eigenvalue. A smaller eigenvalue is associated with a lower SNR. This information has been well-known in the field of principal component analysis. Wernick *et al*. [13] and Wang *et al*. [9][16] have utilized this information for PWLS-based approaches, where the penalty parameter in the PWLS cost function is inversely proportional to the KL eigenvalue. If a PWLS cost function is used for image reconstruction in the KL domain, the cost function minimization will be computed iteratively. Wernick *et al*. [13] explored this kind of iterative PWLS reconstruction on all the KL components after a single KL transform on all phases of a cardiac cycle in dynamic PET (positron emission tomography) and later in gated SPECT (single photon emission computed tomography) [14]. If the KL transform is applied to each phase plus its two nearest neighbors to consider the strongest correlation in order to minimize any possible motion artifact, the iterative PWLS reconstructions will be repeated for each phase and would be time consuming. To reduce the computing burden, we explored an alternative strategy [16] in which the PWLS cost function was used for sinogram restoration in the KL domain and the computation was carried out analytically in a single mathematical operation. The computation was in real time even iterative calculation was used in the sinogram domain. The restored 4D-dCT sinogram was reconstructed by a standard FBP algorithm (i.e., with the Ramp filter at 100% Nyquist frequency cutoff) in a phase-by-phase fashion. Although the PWLS cost function is attractive because of its ability of weighting data differently according to their different statistical significances (i.e., a measurement with higher counts or higher statistical significance is weighted more than a measurement with lower counts or less statistical significance), its outcome may vary depending on the penalty term. An adequate penalty with an appropriate weight would generate a good result. The penalty plays essentially the role of noise reduction while retaining the border details. For FBP

reconstruction of CT images, the filtering step plays the same role of noise reduction while retaining the border details. If the filtering step can be adaptive to the KL eigenvalues, we would avoid the variation of different penalties and retain the high speed of the well-established FBP in CT image reconstruction.

To realize the idea of adaptive FBP reconstruction on different principal components in the KL domain, we selected as an example the cutoff frequency of a well-known low-pass linear filter to be adaptive to the KL eigenvalues. Other possible choices include eigenvalue-adaptive non-linear filters and eigenvalue-adaptive filter-description parameters. For each phase of the 4D-dCT sinogram, we obtained three KL components from the two nearest neighbors plus the concerned one itself by equation (1). Each of these three KL components $\tilde{y}$ was reconstructed by FBP with the cutoff frequency depending on the corresponding KL eigenvalue. After three FBP reconstructions each for one KL component, we performed an inverse KL transform on the reconstructed three KL components to obtain the 3D-CT image at that phase. The same procedure was then repeated to other phases for a fully 4D-dCT image reconstruction. Since the same procedure was applied independently on all the phases, the computation could be parallelized. Each procedure on a phase of the 4D dCT sinogram can be performed on a CPU processor of a multi-CPU platform or a note of a computer cluster.

## III. Results

### *A. Test on a Patient Study:*

In this preliminary study, we tested the effectiveness of the KL-domain adaptive FBP reconstruction by a patient lung scan. The clinical 4D-dCT patient data was acquired by a Discovery ST LightSpeed 8-slice PET/CT scanner (GE Medical Systems) in cine or stop-and-shoot mode [10]. There were multiple rotations at one couch position. The duration time at each couch position was the average respiration cycle plus one second. For example, if the patient respiration period was 4 second, then the duration time was 5 second. The patient was asked to breathe normally during the scan. A plastic block with two infrared reflective markers was taped on the top of the patient's abdomen, placed medially by a few cm inferior to the xiphoid processes. The respiratory signal of the patient from the real-time position management (RPM) system (Varian Medical Systems, Palo Alto, CA) was recorded and synchronized with the CT data acquisition. The axial coverage of the patient was 25 cm. Other scan parameters included 120 kVp, 100 mAs, 0.5 seconds per rotation, 2.5 mm reconstruction of image slice thickness. After the scanned data were prospectively reconstructed at the PET/CT scanner, both the CT images and the corresponding motion data recorded by the RPM system were transferred to a GE Advantage Workstation (GE Medical Systems). The "Advantage 4D" software in the workstation simultaneously displays the CT images and the motion data, and sorts the cine images into a set of respiratory phase images. A total of 10 phases were created, with phase intervals of 10% of the respiratory cycle. Each 3D-CT image at a phase consists of 100 slices each of 512×512 array size.

Since the manufacturer does not allow the raw data or the 4D-dCT sinograms being read out, we have to simulate the sinograms from the sorted cine CT images. The simulation was based on the CT scanner geometry. Each detector slice or band consists of an array of 888 cells which are on an arc concentric to the X-ray source with a distance of 949.075 mm. The distance from the rotation center to the X-ray source is 541 mm. The detector cell spacing is 1.0239 mm. A 2D sinogram was simulated from each image slice in fan-beam geometry. A total of 984 projection angles or views were taken evenly spanned on a circular orbit of $360^{o}$. Each re-projected dataset consists of 888 samples from the corresponding 888 detector cells. Each line integral was calculated based on the Siddon's ray-tracing technique [17] between the X-ray source point and the center of the detector cell. The intersecting length of the ray with a square image pixel was used as the weight of the pixel's contribution to the line integral.

To show the characteristics of the KL transform on the nearest neighboring phases, a simulated 2D sinogram was directly reconstructed by a standard FBP algorithm (i.e., by the use of the Ramp filer at 100% Nyquist frequency) as the reference. In order to avoid the non-uniform noise propagation problem in fan-beam image reconstruction, the intersecting area of fan-beam strip and square image pixel was used as the weight, rather than a bi-linear interpolation, in the backprojection step in the fan-beam FBP algorithm [18]. The result is shown by Figure 1(a). After applying the KL transform on the 2D sinogram and its two nearest neighboring phases, the same FBP algorithm was used to reconstruct all the three principal components in the KL domain. Then the three reconstructed principal components were subjected to an inverse KL transform for the final CT images. These three CT images are shown by Figure 1(b), 1(c) and 1(d), respectively. It can be observed that the first KL component contains almost all the information (i.e., very similar to the reference of Figure 1(a)), while the second and third KL components are dominated by noise and artifacts. Therefore, the cutoff frequency in the filtering step of the FBP reconstruction on the second or third component shall be noticeably different from that on the first component, i.e., the cutoff frequency shall be chosen to reflect different SNRs of different KL components.

To show the difference between a low-pass filter with a fixed cutoff frequency and with an adaptive frequency to each KL component, we selected the low-pass Butterworth filter as an example. The cutoff frequency for the second-order Butterworth filter was chosen to be proportional to the fourth root of the corresponding eigenvalue. The reconstruction

procedure used for Figure 1(b)-(d) was repeated with the adaptive Butterworth filter and the obtained final result after inverse KL transform is shown by Figure 2(a). The reconstruction procedure was also repeated with the Butterworth filter at a fixed frequency to all the three KL components. By an error-and-trial fashion, we found a fixed frequency at 70% Nyquist frequency which produced the visually best reconstruction among others in the range from 25% up to 100% Nyquist frequency. The result is shown by Figure 2(b). It can be observed that the adaptive FBP strategy shows a lightly better reconstruction than the fixed cutoff frequency FBP algorithm in terms of noise suppression. Since the patient scan was acquired by a relatively high mAs parameter, the noise level is relatively low and the visual difference is small between the fixed and adaptive FBP reconstructions. To further see their difference, we performed a quantitative study below.

### *B. Noise-Resolution Tradeoff Measurement*

The noise-resolution tradeoff merit was chosen to measure quantitatively the difference between the fixed and adaptive FBP reconstructions. The resolution was characterized by an edge spread function (ESF) along a sharp edge (the hot spot on the right of the heart) in the reconstructed CT image in Figure 2(a) and 2(b) respectively. The broadening of the ESF reflects the resolution of the reconstructed image. The noise level was characterized by the variance of a uniform area around the selected edge (lower left and upper right of the hot spot). By varying the cutoff frequency of the Butterworth filter during FBP reconstruction, we obtained the noise-resolution curves as shown in Figure 3. For the adaptive filtering, the fourth-root proportional relationship to the KL eigenvalue remained the same when the cutoff frequency on the first KL component varied. In other words, when the cutoff frequency on the first KL component varied, the cutoff frequencies for the second and third components varied accordingly. The gain of the KL-domain adaptive FBP strategy is observed at all resolution range.

## IV. Conclusion

In this work, we reported a new analytical reconstruction strategy for 4D-dCT, i.e., a KL-domain adaptive FBP reconstruction method. The strategy was based on the observation that there are strong signal correlations among different phases of the 4D-dCT dataset and the KL transform provides a unique means to de-correlate the signals and rearrange the data according their SNRs or eigenvalues. For the KL component associated with a smaller eigenvalue, a stronger smoothing criterion should be applied for heavier noise suppression. This idea was realized as an example by setting the cutoff frequency of a low-pass filter adaptive to the eigenvalue during FBP reconstruction of the KL components in the KL domain. The gain of the KL-domain adaptive FBP reconstruction was quantitatively demonstrated by a noise-resolution tradeoff study.

This adaptive FBP strategy is different from the previous approaches [12]-[15]. The previous approaches apply the KL transform to all the phases during a complete cardiac cycle. This adaptive FBP strategy is also different from our previous work [16]. Although it applies the KL transform to the nearest neighboring phases for adaptive noise reduction on each principal component by a PWLS sinogram restoration in the KL domain, the previous work [16] reconstructs the 4D-dCT image sequence in the image domain by a fixed frequency FBP algorithm in a frame-by-frame reconstruction fashion. It would be an interesting topic to compare this presented adaptive FBP strategy with our previous work [16].

## V. References


[1] D.A. Low, M. Nystrom, E. Kalinin, P. Parikh, J.F. Dempsey, J.D. Bradley, S. Mutic, S.H. Wahab, T. Islam, G. Christensen, D.G. Politte, and B.R. Whiting, "A method for the reconstruction of 4-dimensional synchronized CT scans acquired during free breathing", *Medical Physics*, vol. 30, pp. 1254-1263, 2003.

[2] P.J. Keall, G. Starkschall, H. Shukla, K.M. Forster, V. Ortiz, C. W. Stevens, S.S. Vedam, R. George, T. Guerrero, and R. Mohan, "Acquiring 4D thoracic CT scans using a multislice helical method", *Phys. Med. Biol.*, vol. 49, pp. 2053-2067, 2004.

[3] T. Pan, T.Y. Lee, E. Rietzel, and G.T.Y. Chen, "4D-CT imaging of a volume influenced by respiratory motion of multi-slice CT", *Medical Physics*, vol. 31, pp. 333-340, 2004.

[4] J. Hsieh, "Adaptive streak artifact reduction in computed tomography resulting from excessive X-ray photon noise", *Medical Physics*, vol. 25, pp. 2139-2147, 1998.

[5] M. Kachelrieβ, O. Watzke, and W.A. Kalender, "Generalized multi-dimensional adaptive filtering for conventional and spiral single-slice, multi-slice, and cone-beam CT", *Medical Physics*, vol. 28, pp. 475-490, 2001.

[6] J. Zhong, R. Ning, and D. Conover, "Image denoising based on multiscale singularity detection for cone beam CT breast imaging", *IEEE Trans. Medical Imaging*, vol. 23, pp. 696-703, 2004.

[7] P.J. La Rivière, "Penalized-likelihood sinogram smoothing for low-dose CT", *Medical Physics*, vol. 32, pp. 1676-1683, 2005.

[8] T. Li, X. Li, J. Wang, J. Wen, H. Lu, J. Hsieh, and Z. Liang, "Nonlinear sinogram smoothing for low-dose X-ray CT", *IEEE Trans. Nuclear Science*, vol. 51, pp. 2505-2513, 2004.

[9] J. Wang, T. Li, H. Lu, and Z. Liang, "Penalized weighted least-squares approach to sinogram noise reduction and image reconstruction for low-dose X-ray computed tomography", *IEEE Trans. Medical Imaging*, vol. 25, pp. 1272-1283, 2006.

[10] T. Li, B. Schreibmann, B. Thorndyke, G. Tillman, A. Boyer, and L.Xing, "Radiation dose reduction in four-dimensional computed tomography," *Medical Physics*, vol. 32, pp. 3650–3660, 2005.

[11] T. Li, A. Koong, and L. Xing, "Enhanced 4D cone-beam CT with inter-phase motion model", *Medical Physics*, vol. 34, pp. 3688-3695, 2007.

[12] C-M. Kao, J.T. Yap, J. Mukherjee, and M.N. Wernick, "Image reconstruction for dynamic PET based on low-order

approximation and restoration of the sinogram", *IEEE Trans. Medical Imaging*, vol. 16, pp. 738-749, 1997.

[13] M.N. Wernick, E.J. Infusino, and M. Milošević, "Fast spatio-temporal image reconstruction for dynamic PET", *IEEE Trans. Medical Imaging*, vol. 18, pp. 185-195, 1999.

[14] M.V. Narayanan, M.A. King, M.N. Wernick, C.L. Byrne, E.J. Soares, and P.H. Pretorius, "Improved image quality and computation reduction in 4-D reconstruction of cardiac-gated SPECT images", *IEEE Trans. Medical Imaging*, vol. 19, pp. 423-433, 2000.

[15] H. Lu, G. Han, D. Chen, L. Li, and Z. Liang, "A theoretically based pre-reconstructing filter for spatio-temporal noise reduction in gated cardiac SPECT imaging", *Conf Record IEEE NSS-MIC*, in CD-ROM, 2000.

[16] J. Wang, T. Li, H. Lu, and Z. Liang, "Noise reduction for four dimensional computed tomography", *The 9th International Meeting on Fully Three-Dimensional Image Reconstruction in Radiology and Nuclear Medicine*, pp. 441-444, 2007.

[17] R. Siddon, "Fast calculation of the exact radiological path for a three-dimensional CT array", *Medical Physics*, vol. 12, pp. 252-253, 1986.

[18] J. Wang, H. Lu, T. Li, and Z. Liang, "An alternative solution to the non-uniform noise propagation problem in fan-beam FBP image reconstruction", *Medical Physics*, vol. 32, pp. 3389-3394, 2005.

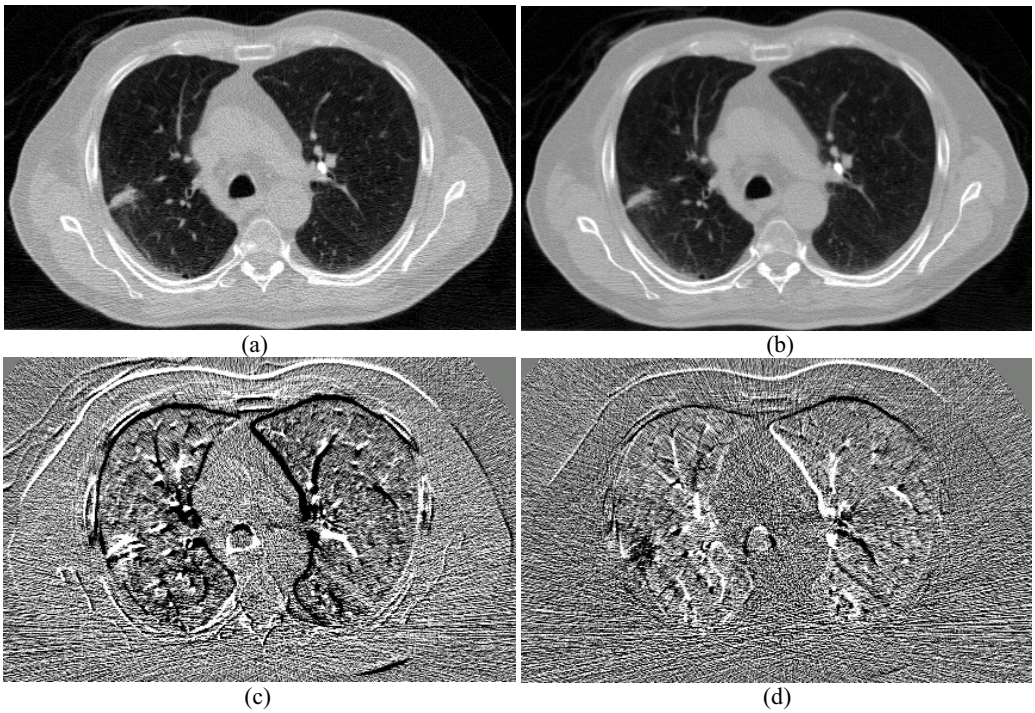

(a) (b) (c) (d)

Figure 1: Illustration of one slice of reconstructed CT image: (a) standard FBP (with Ramp filter at 100% Nyquist frequency cutoff) frame-by-frame reconstruction; (b) standard FBP from the first KL component; (c) standard FBP from the second KL component; (d) standard FBP from the third KL component; (e) direct FBP (frame-by-frame) using Butterworth filter at 70% Nyquist frequency cutoff; and (f) the KL-domain FBP using Butterworth filter with cutoff frequency adaptive to the KL eigenvalues. The eigenvalues of these three KL components are $2.92 \times 10^{10}$, $1.94 \times 10^{7}$ and $1.50 \times 10^{7}$.

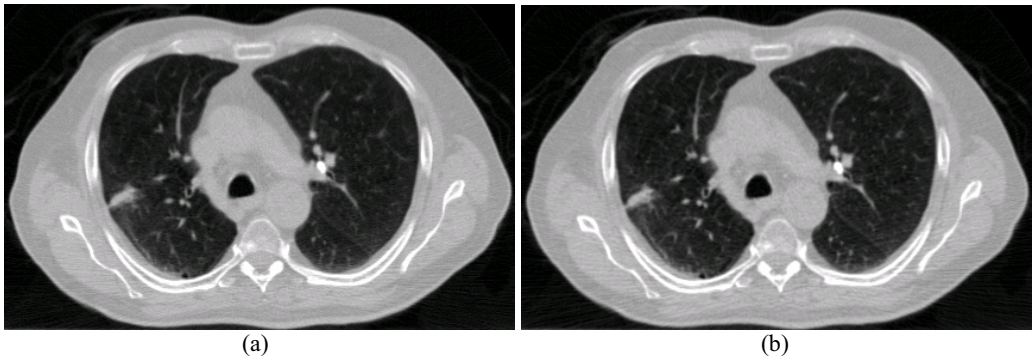

(a) (b)

Figure 2: (a) Direct FBP (frame-by-frame) using Butterworth filter at 70% Nyquist frequency cutoff; and (b) the KL-domain FBP using Butterworth filter with cutoff frequency adaptive to the KL eigenvalues.

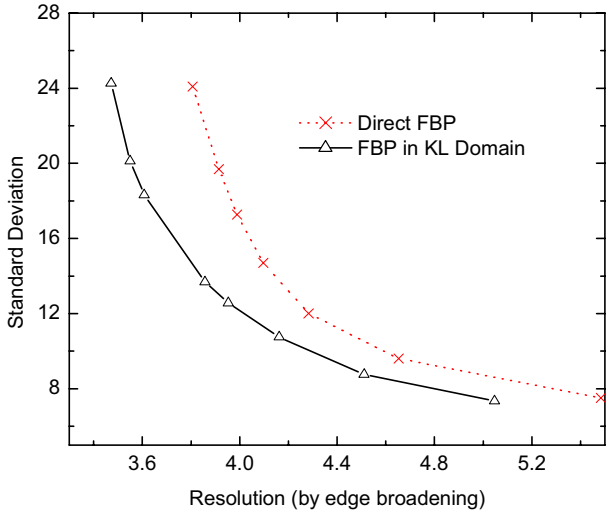


Figure 3: Noise-resolution tradeoff curves for the direct FBP and the K L-domain adaptive FBP reconstruction of 4D datasets.